Wireless channel Rank Enhancement via RIS-assited Communications System

Contents

Abstract

The abstract goes here.

25
26

Index haye shakhsi

Index Terms

IEEE, IEEEtran, journal, LATEX, paper, template.

I. Introduction

Gramma check start

AS wireless communication systems shift to higher frequency bands, they encounter challenges including significant path loss, increased system complexity, and reduced channel coherence. To mitigate these issues, innovative technologies like Reconfigurable Intelligent Surfaces (RIS) have emerged as potential solutions. In this article, we explore the fundamental principles and performance of these reconfigurable surfaces.

II. Understanding the Principals

In conventional communications systems, performance and quality improvements were typically achieved by modifying the transmitter or receiver. The wireless channel has traditionally behaved stochastically. Recently, a promising technology, Reconfigurable Intelligent Surfaces, has emerged, allowing communications systems to manipulate the channel itself, similar to how transmitters and receivers are controlled [1].

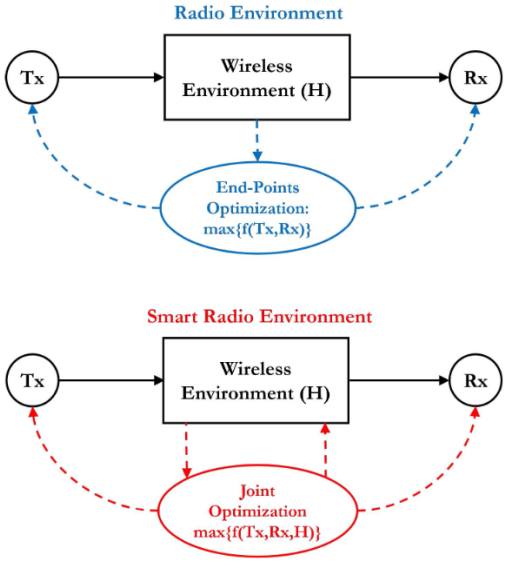

Figure 1: Smart Radio Environment(SRE)

A. How it works

RISs are composed of hundreds of PIN diodes, each capable of adjusting the phase, amplitude, and polarization of an incident wave [2]. This enables RISs to alter the properties of the reflected wave toward the receiver by utilizing non-line-of-sight paths and beamforming to steer the beam in a specific direction. The term 'passive' can be misleading, as the surfaces employ active diodes to control the phase. In real-world scenarios, we must consider a power consumption of approximately 0.33 milliwatts(mW) [3] and $50\mu W$ [4] per diode. For instance, a RIS controller with 256 elements consumes about 0.72 W [3].

B. Continuous vs. Discrete phase-shift

The RIS needs to align the beamforming through optimal phase shifts. Due to the high complexity of continuous phase-shift algorithms, a new approach called discrete phase-shift optimization was introduced in [5]. The results indicate that discrete phase shifts can asymptotically achieve the same performance as continuous phase shifts when a large number of elements is used. To elaborate on this concept, it is beneficial to examine 2 given in [5]. Likewise, some information is gathered in the I."

Table I: The Power Loss of Using IRS with Discrete Phase Shifts

Number of control bits: b	$b=1$	$b=2$	$b=3$	$b=\infty$ (continuous phase shifts)
Power loss: $\frac{1}{\left(\frac{2^b}{\pi}\sin\left(\frac{\pi}{2^b}\right)\right)^2}$	3.9 dB	0.9 dB	0.2 dB	0 dB

C. Channel Model and Properties

Several channel modeling approaches have been used for the RIS-aided systems. Generally, the direct path is considered as a Rayleigh fading distribution due to isotropic scattering assumptions [6], [7].

$l \sim \mathcal{N}_{\mathbb{C}}(0, \beta)$, where β is the variance of the noise distribution. The RIS surface contains $N = N_H * N_V$ elements, which are spread as a Uniform Planar Array (UPA), and antenna arrays are located as a Uniform Linear Array (ULA).

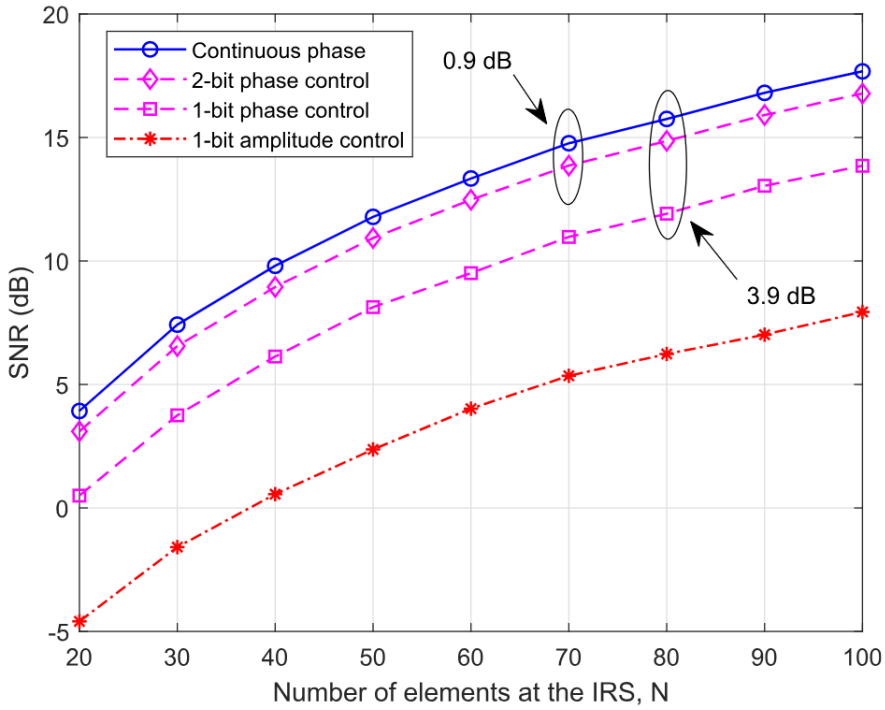

Figure 2: Comparison between discrete and continuous phase-shifts Vs. number of elements

1) Modeling ULA
Assume we have the array shape 3
[8]

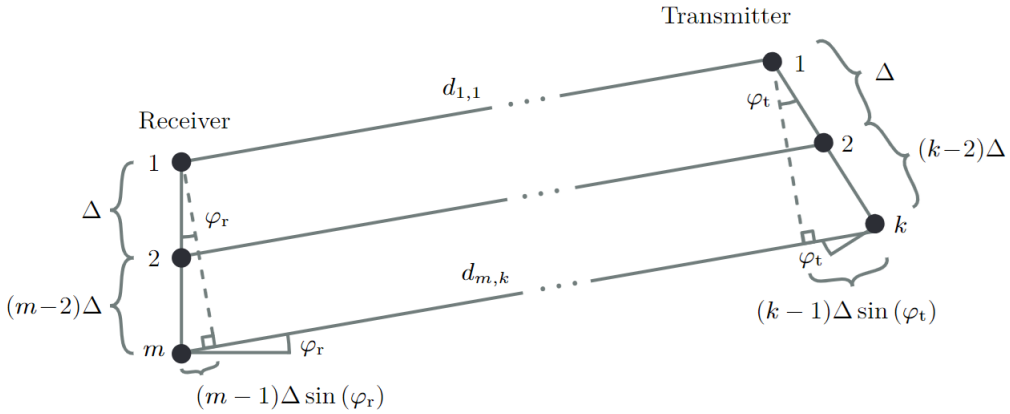

Figure 3: Array response basic scheme

The far-field region is defined for $d \geq 2M^2\Delta^2/\lambda$ and $d \geq 2K^2\Delta^2/\lambda$. The distance for each element is given by

$$d_{m,k} = d + (k-1)\Delta\sin(\varphi_t) + (m-1)\Delta\sin(\varphi_r), \tag{1}$$

The channel gain for far-field assumption always defines as

$$\beta = \frac{\lambda^2}{(4\pi)^2}\frac{1}{d_{m,k}^2}, \tag{2}$$

To compose a channel we follow on 3

$$h_{m,k} = \sqrt{\beta_{m,k}}e^{-j2\pi\frac{(d_{m,k}-d)}{\lambda}}, \tag{3}$$

Generally, shaping the Channel matrix for all involved elements and arrays is formed

$$\mathbf{H} = \begin{bmatrix} h_{1,1} & \dots & h_{1,K} \\ \vdots & \ddots & \vdots \\ h_{M,1} & \dots & h_{M,K} \end{bmatrix} = \begin{bmatrix} \sqrt{\beta_{1,1}} e^{-j2\pi \frac{(d_{1,1}-d)}{\lambda}} & \dots & \sqrt{\beta_{1,K}} e^{-j2\pi \frac{(d_{1,K}-d)}{\lambda}} \\ \vdots & \ddots & \vdots \\ \sqrt{\beta_{M,1}} e^{-j2\pi \frac{(d_{M,1}-d)}{\lambda}} & \dots & \sqrt{\beta_{M,K}} e^{-j2\pi \frac{(d_{M,K}-d)}{\lambda}} \end{bmatrix}. \tag{4}$$

Substituting 1 and expanding the 4 yield in

$$\begin{aligned} \mathbf{H} = \begin{bmatrix} h_{1,1} & \cdots & h_{1,K} \\ \vdots & \ddots & \vdots \\ h_{M,1} & \cdots & h_{M,K} \end{bmatrix} &= \sqrt{\beta} \begin{bmatrix} 1 & \cdots & e^{-j2\pi \frac{(K-1)\Delta}{\lambda} \sin(\varphi_t)} \\ \vdots & \ddots & \vdots \\ e^{-j2\pi \frac{(M-1)\Delta}{\lambda} \sin(\varphi_r)} & \cdots & e^{-j2\pi \frac{(M-1)\Delta}{\lambda} \sin(\varphi_r)} e^{-j2\pi \frac{(K-1)\Delta}{\lambda} \sin(\varphi_t)} \end{bmatrix} \\ &= \sqrt{\beta} \begin{bmatrix} 1 & \cdots & e^{-j2\pi \frac{(K-1)\Delta}{\lambda} \sin(\varphi_t)} \\ \vdots & \ddots & \vdots \\ e^{-j2\pi \frac{(M-1)\Delta}{\lambda} \sin(\varphi_r)} & \cdots & e^{-j2\pi \frac{(M-1)\Delta}{\lambda} \sin(\varphi_r)} \end{bmatrix} \begin{bmatrix} 1 & \cdots & e^{-j2\pi \frac{(K-1)\Delta}{\lambda} \sin(\varphi_t)} \end{bmatrix}, \end{aligned} \tag{5}$$

It can be rewritten as a shortened expression, representing 2-ULAs formula

$$\mathbf{H} = \sqrt{\beta} \mathbf{a}_M(\varphi_r) \mathbf{a}_K^T(\varphi_t). \tag{6}$$

2) Modeling UPA

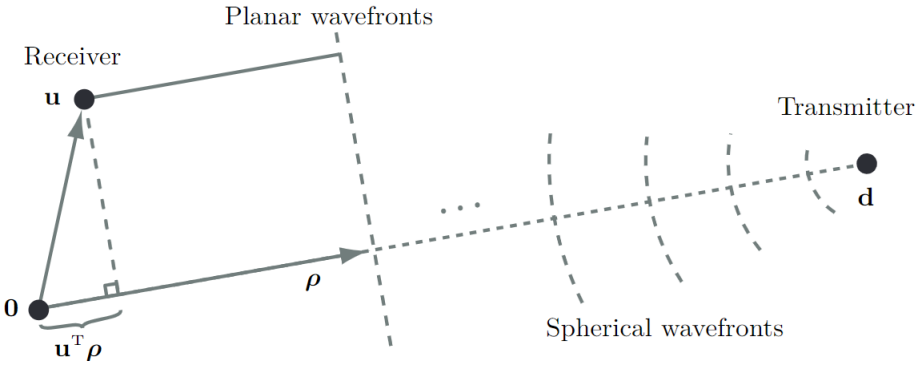

Figure 4: Two elements UPA in 3-D

$$
\begin{aligned}
\mathbf{a}_{M_H,M_V}(\varphi,\theta) &= \begin{bmatrix} 1 \\ e^{-j\frac{2\pi}{\lambda}(i(2)\Delta\sin(\varphi)\cos(\theta)+j(2)\Delta\sin(\theta))} \\ \vdots \\ e^{-j\frac{2\pi}{\lambda}(i(M)\Delta\sin(\varphi)\cos(\theta)+j(M)\Delta\sin(\theta))} \end{bmatrix} \\
&= \begin{bmatrix} 1\cdot\begin{bmatrix} 1 \\ e^{-j2\pi\frac{\Delta\sin(\varphi)\cos(\theta)}{\lambda}} \\ \vdots \\ e^{-j2\pi\frac{(M_H-1)\Delta\sin(\varphi)\cos(\theta)}{\lambda}} \end{bmatrix} \\ e^{-j2\pi\frac{\Delta\sin(\theta)}{\lambda}}\cdot\begin{bmatrix} 1 \\ e^{-j2\pi\frac{\Delta\sin(\varphi)\cos(\theta)}{\lambda}} \\ \vdots \\ e^{-j2\pi\frac{(M_H-1)\Delta\sin(\varphi)\cos(\theta)}{\lambda}} \end{bmatrix} \\ \vdots \\ e^{-j2\pi\frac{(M_V-1)\Delta\sin(\theta)}{\lambda}}\cdot\begin{bmatrix} 1 \\ e^{-j2\pi\frac{\Delta\sin(\varphi)\cos(\theta)}{\lambda}} \\ \vdots \\ e^{-j2\pi\frac{(M_H-1)\Delta\sin(\varphi)\cos(\theta)}{\lambda}} \end{bmatrix} \end{bmatrix} \\
&= \begin{bmatrix} 1\cdot\mathbf{a}_{M_H}(\varphi,\theta) \\ e^{-j\frac{2\pi\Delta\sin(\theta)}{\lambda}}\cdot\mathbf{a}_{M_H}(\varphi,\theta) \\ \vdots \\ e^{-j\frac{2\pi(M_V-1)\Delta\sin(\theta)}{\lambda}}\cdot\mathbf{a}_{M_H}(\varphi,\theta) \end{bmatrix} = \mathbf{a}_{M_V}(\theta,0)\otimes\mathbf{a}_{M_H}(\varphi,\theta)
\end{aligned} \tag{7}
$$

In ro az maghale emil arrange konim tozih zarb kronecker

In order to define the general array response, we first need to define the basis vector.

The general distance-dependent path loss model [9] is presented as:

$$L(d) = C_0\left(\frac{d}{D_0}\right)^{-\alpha}, \tag{8}$$

in case of considering small-scale fading the above formula [9] can be shaped as

$$\mathbf{H} = \sqrt{\frac{\beta_{AI}}{1+\beta_{AI}}}\mathbf{H}_{\text{LoS}} + \sqrt{\frac{1}{1+\beta_{AI}}}\mathbf{H}_{\text{NLoS}}, \tag{9}$$

another modeling consists of all the NLOS and LOS rays [10]

3) Modeling 3-D Far-field channel

Defining the transmitter's location as $d \in \mathbb{R}^3$ helps in establishing our formulation. Next, we define the unit-length vector as

$$\rho = \frac{d}{\|d\|} \tag{10}$$

Likewise, we can define this vector in the spherical coordination as

$$\rho = \begin{bmatrix} \cos(\varphi)\cos(\theta) \\ \sin(\varphi)\cos(\theta) \\ \sin(\theta) \end{bmatrix} \tag{11}$$

The location of the other receiving antenna element, as shown in 4, is denoted by $u \in \mathbb{R}^3$. Additionally, the indexing function for the horizontal and vertical axes of the array m is characterized as follows:

$$i(m) = (m-1) - M_H \left\lfloor \frac{m-1}{M_H} \right\rfloor \in \{0, 1, \ldots, M_H - 1\}, \tag{12}$$

$$j(m) = \left\lfloor \frac{m-1}{M_H} \right\rfloor \in \{0, 1, \ldots, M_V - 1\}, \tag{13}$$

To ensure a consistent projection, we define the location vector as

$$\mathbf{u}_m = \begin{bmatrix} 0 \\ -i(m)\Delta \\ -j(m)\Delta \end{bmatrix}. \tag{14}$$

While the corresponding phase shift is

$$-\frac{2\pi}{\lambda}\mathbf{u}^T\boldsymbol{\rho} \tag{15}$$

$$\mathbf{u}_m^T\boldsymbol{\rho} = \begin{bmatrix} 0 \\ -i(m)\Delta \\ -j(m)\Delta \end{bmatrix}^T \begin{bmatrix} \cos(\varphi)\cos(\theta) \\ \sin(\varphi)\cos(\theta) \\ \sin(\theta) \end{bmatrix} = -i(m)\Delta\sin(\varphi)\cos(\theta) - j(m)\Delta\sin(\theta). \tag{16}$$

$$\mathbf{H} = \sqrt{\beta_{\text{iso}}}\sqrt{G_t(\varphi_t, \theta_t)}\sqrt{G_r(\varphi_r, \theta_r)}\mathbf{a}_M(\varphi_r, \theta_r)\mathbf{a}_K^T(\varphi_t, \theta_t). \tag{17}$$

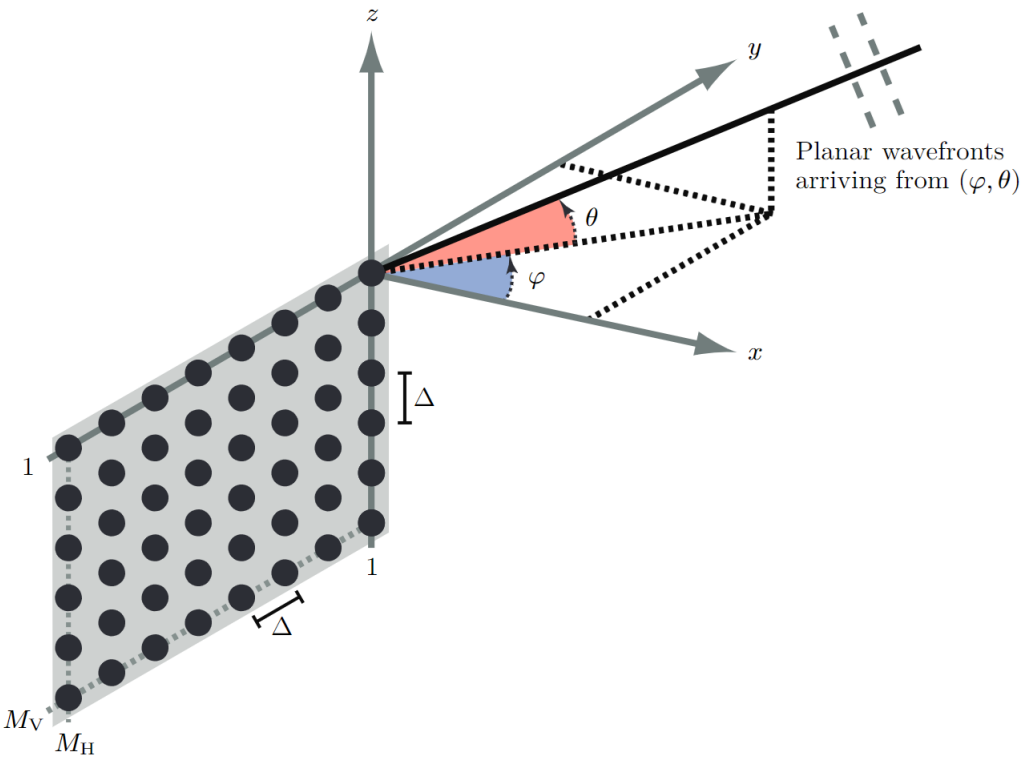

Figure 5: UPA and indexing

D. Clustered Multipath Propagation

[8]

$$\mathbf{h} = \sum_{i=1}^{N_{\text{cl}}} \left(\sum_{n=1}^{N_{\text{path}}} \alpha_{i,n} e^{-j\psi_{i,n}} \right) \mathbf{a}(\varphi_i, \theta_i). \tag{18}$$

$$\mathbb{E}\left\{\alpha_{i,n}^2\right\} = \frac{\beta_i}{N_{\text{path}}}. \tag{19}$$

$$\sum_{n=1}^{N_{\text{path}}} \alpha_{i,n} e^{-j\psi_{i,n}} \to \mathcal{N}_{\mathbb{C}}(0, \beta_i) \tag{20}$$

$$\mathbf{h} = \sum_{i=1}^{N_{\text{cl}}} c_i \mathbf{a}(\varphi_i, \theta_i). \tag{21}$$

$$\mathbf{h} \sim \mathcal{N}_{\mathbb{C}}(0, \mathbf{R}_h), \tag{22}$$

$$\mathbf{R}_h = \mathbb{E}\{\mathbf{h}\mathbf{h}^H\} = \sum_{i=1}^{N_{\text{cl}}} \sum_{n=1}^{N_{\text{cl}}} \mathbb{E}\{c_i c_n^*\} \mathbf{a}(\varphi_i, \theta_i) \mathbf{a}^H(\varphi_n, \theta_n) = \sum_{i=1}^{N_{\text{cl}}} \beta_i \mathbf{a}(\varphi_i, \theta_i) \mathbf{a}^H(\varphi_i, \theta_i). \tag{23}$$

$$\mathbf{R}_h = \beta \int_{-\pi}^{\pi} \int_{-\pi/2}^{\pi/2} f_{\varphi,\theta}(\varphi, \theta) \mathbf{a}(\varphi, \theta) \mathbf{a}^H(\varphi, \theta) \, \mathrm{d}\theta \mathrm{d}\varphi, \tag{24}$$

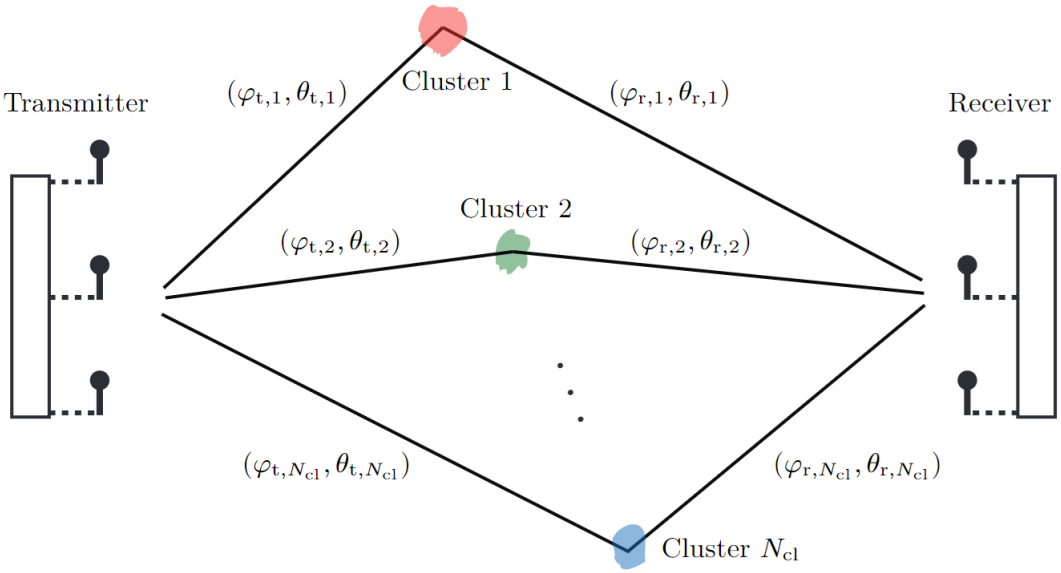

Figure 6: clustered channel

$$\mathbf{H} = \sum_{i=1}^{N_{\text{cl}}} c_i \mathbf{a}_M(\varphi_{r,i}, \theta_{r,i}) \mathbf{a}_K^{\mathsf{T}}(\varphi_{t,i}, \theta_{t,i}), \tag{25}$$

$$\mathbf{H} = \sum_{i=1}^{N_{cl}} c_i \sqrt{G_t(\varphi_{t,i}, \theta_{t,i}) G_r(\varphi_{r,i}, \theta_{r,i})} \mathbf{a}_M(\varphi_{r,i}, \theta_{r,i}) \mathbf{a}_K^{\top}(\varphi_{t,i}, \theta_{t,i}) \tag{26}$$

$$\bar{c}_i = c_i \sqrt{G_t(\varphi_{t,i}, \theta_{t,i}) G_r(\varphi_{r,i}, \theta_{r,i})} \sim \mathcal{N}_{\mathbb{C}}\left(0, \bar{\beta}_i\right) \tag{27}$$

E. Multiplicative fading

In many scenarios, the direct path is strong; consequently, the conventional RIS is unable to achieve the desired performance [11]. Another issue with the conventional RIS can be understood through the multiplicative path-loss formula.

$$\mathbb{E}\left\{|G|^2\right\} = \sigma_G^2 \propto \frac{1}{d_G^{\alpha_g}}, \tag{28}$$

$$\mathbb{E}\left\{|H|^2\right\} = \sigma_H^2 \propto \frac{1}{d_H^{\alpha_h}}, \tag{29}$$

Because the two paths are independent, the cascaded channel gain is proportional to

$$\mathbb{E}\{|H_n G_n|^2\} = \sigma_H^2 \sigma_G^2 \propto \frac{1}{d_H^{\alpha_h} d_G^{\alpha_g}}. \tag{30}$$

To overcome the aforementioned problems, a new type of RIS has emerged, known as Active RIS [2]. Active RIS allows for amplification while reflecting the incident wave.

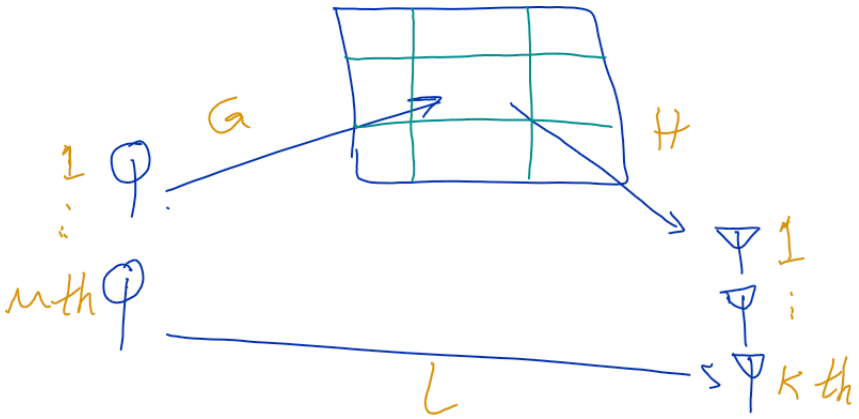

Figure 7: RIS-aided MIMO communcaiton system

III. SYSTEM MODEL

A. The Basic diagrams of the RIS-aided communication system

The channels for AP-RIS, RIS-User, and the direct channel are denoted by $\mathbf{G} \in \mathbb{C}^{N\times M}, \mathbf{H} \in \mathbb{C}^{k\times N}$, and $\mathbf{L} \in \mathbb{C}^{k\times M}$, respectively. Let $\boldsymbol{\theta} = [\theta_1, \theta_2, ..., \theta_N]$ and define a phase-shift matrix as $\boldsymbol{\Theta} = \text{diag}(\beta_1 e^{j\theta_1}, \ldots, \beta_N e^{j\theta_N})$ where we can observe the system setup in figure 7

B. Practical Channel Modeling

Here's a revised version of your text for improved clarity and readability:

Due to the presence of thousands of RIS elements, the number of channels is proportional to $\mathcal{O}(MNK)$. As a result, simulating the channel in matrix form is more practical. One of the prominent approaches for simulation is array response channel modeling. Uniform Linear Arrays (ULA) and Uniform Planar Arrays (UPA) are commonly used to account for phase shifts across different propagation paths, which result from variations in distance

These surfaces operate under the assumption that Channel State Information (CSI) is availableHowever, estimating all the channels for systems with thousands of RIS elements significantly increases the channel estimation overhead. Consequently, system complexity escalates when employing multiple RISs

The basic function of these diodes is illustrated in 8.

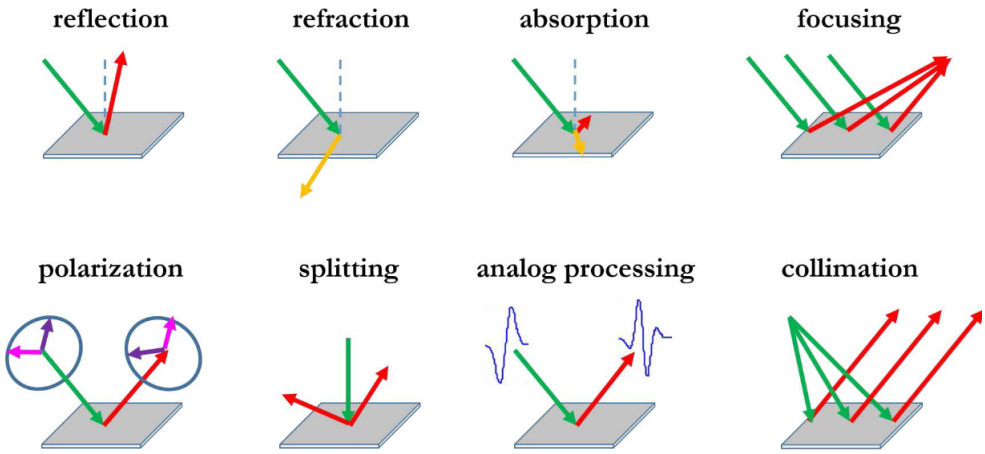

Figure 8: Electromagnetic-based elementary functions.

The array response in 3-D defines as

$$\mathbf{a}(\varphi,\theta) = \left[e^{j\mathbf{k}(\varphi,\theta)^{\mathrm{T}}\mathbf{u}_1}, \ldots, e^{j\mathbf{k}(\varphi,\theta)^{\mathrm{T}}\mathbf{u}_N}\right]^{\mathrm{T}} \tag{31}$$

where $k(\varphi,\theta) \in \mathbb{R}^3$ is the wave vector.

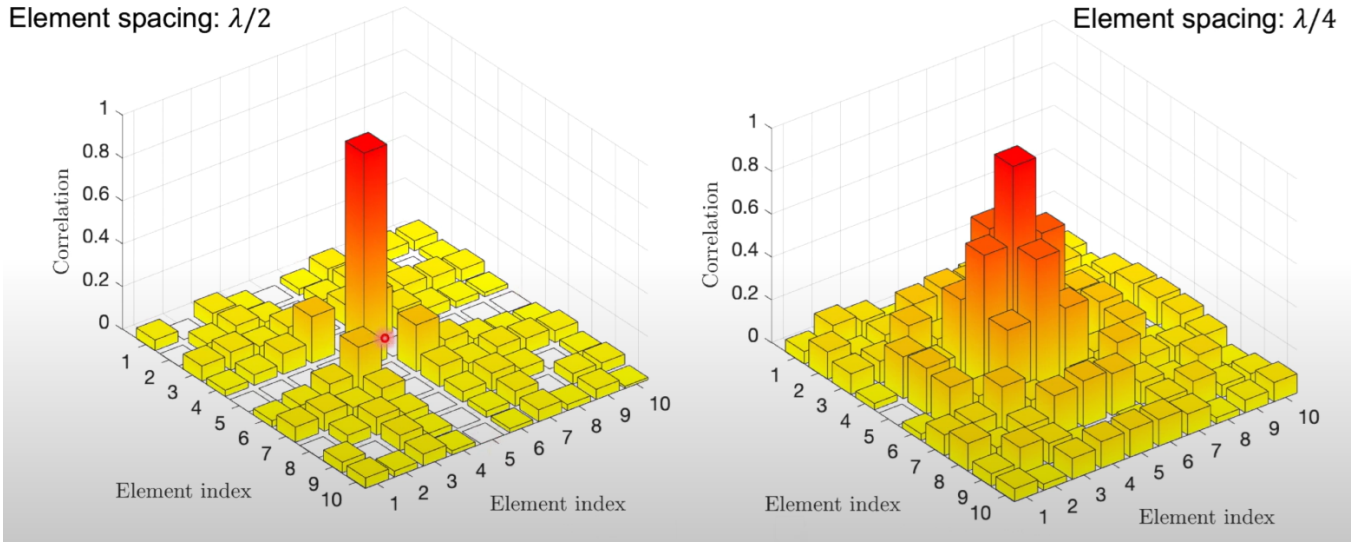

Figure 9: Correlations of RIS elements

$$\mathbf{k}(\varphi,\theta) = \frac{2\pi}{\lambda}\left[\cos(\theta)\cos(\varphi), \quad \cos(\theta)\sin(\varphi), \quad \sin(\theta)\right]^{\mathrm{T}}. \tag{32}$$

In the Rayleigh fading channel model, there are an infinite number of multipaths. However, we begin by considering L impinging plane waves [6]. The channel can be represented as

$$\mathbf{h}_1 = \sum_{l=1}^{L} \frac{c_l}{\sqrt{L}} \mathbf{a}(\varphi_l, \theta_l) \tag{33}$$

where $\frac{c_l}{\sqrt{L}} \in \mathbb{C}$ represents the complex signal attenuation of the lth path, φ_l denotes the azimuth angle of arrival, and θ_l denotes the elevation angle of arrival. By writing down the expectation and simplifying, the correlation between elements yields

$$\begin{aligned}
[\mathbf{R}]_{n,m} &= \int_{-\pi/2}^{\pi/2}\int_{-\pi/2}^{\pi/2} e^{j\frac{2\pi}{\lambda}\|\mathbf{u}_n-\mathbf{u}_m\|\sin(\theta)} f(\varphi,\theta) d\theta d\varphi \\
&= \int_{-\pi/2}^{\pi/2} e^{j\frac{2\pi}{\lambda}\|\mathbf{u}_n-\mathbf{u}_m\|\sin(\theta)} \frac{\cos(\theta)}{2} d\theta \\
&= \frac{\sin\left(\frac{2\pi}{\lambda}\|\mathbf{u}_n-\mathbf{u}_m\|\right)}{\frac{2\pi}{\lambda}\|\mathbf{u}_n-\mathbf{u}_m\|}
\end{aligned} \tag{34}$$

Last but not least, the equation 34 is illustrated in 9. From the eigenvalue perspective of all channels which are generated by the RIS, is depicted in figure 10.

C. MIMO Capacity evaluation

In reference [12], the authors propose the condition number metric to evaluate rank deficiency in MIMO communication. Moreover, this metric is applied to various scenarios, such as optimized RIS placement, antenna array size, and modulation schemes. For instance, they illustrate the condition number versus the location of the RIS in 11, where the intensity represents the condition number, which is formulated as

$$\text{Reciprocal condition number} = \frac{\lambda_2}{\lambda_1}. \tag{35}$$

The rcond is close to 1 if the overall channel H is well-conditioned, whereas the rcond approaches zero if the channel is rank-deficient. In conclusion, areas with rank deficiency are suitable for placing the RIS in the environment.

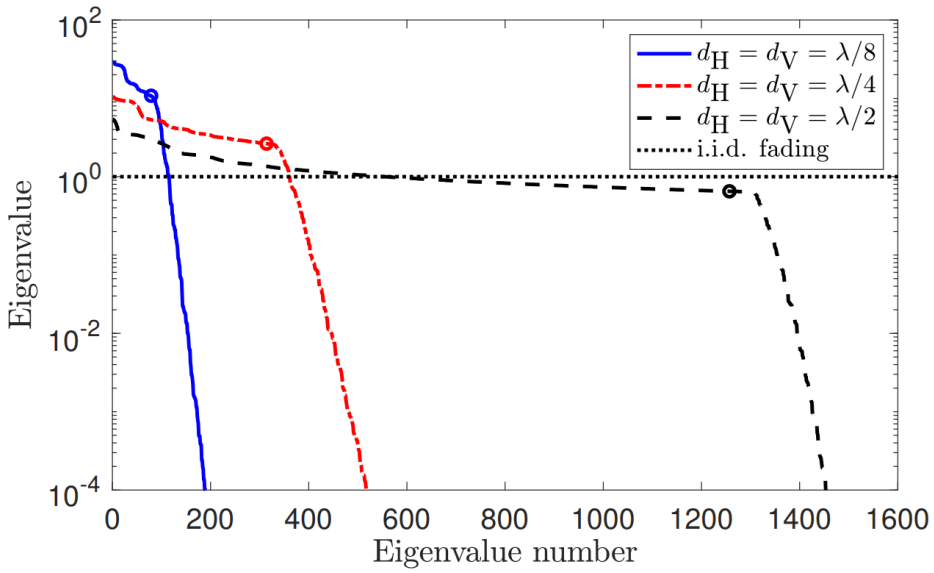

Figure 10: The eigenvalues of R in decreasing order for an RIS with N = 1600 and $d_H = d_V = d \in \frac{\lambda}{8}, \frac{\lambda}{4}, \frac{\lambda}{2}$

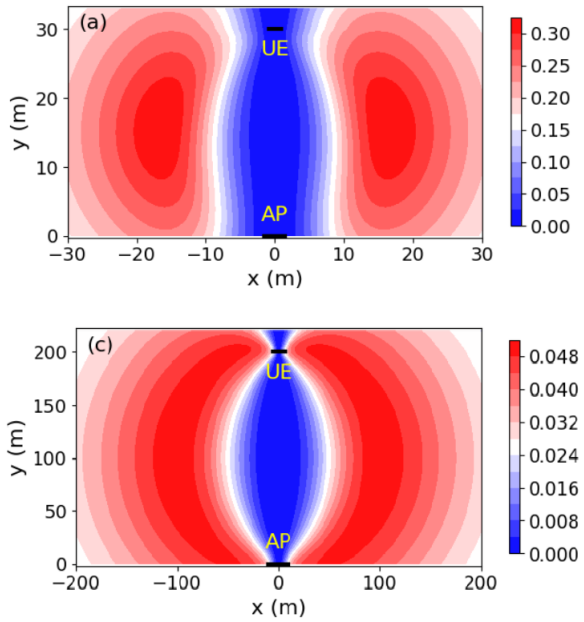

Figure 11: Contours of reciprocal condition number with horizontal distance between AP and UE d = 30m (a) and 200m (b). The solid black lines indicate the locations and orientations of AP and UE, but not represent the actual size of the antenna arrays.

D. Definition of channel hardening and favorable propagation properties

Referencing to [13], the author tries to introduce **FavorablePropagation**, channel hardening, and rank deficiency, which are conceptualized through a stochastic perspective. The channel offers the favorable propagation property if the inner product of two arbitrary channel vectors z_k z_l, $k \neq l$, satisfies

$$z_k^H z_l = 0 \tag{36}$$

which is a strict condition to hold. Thus, the relaxed form is written as $M, N \to \infty$ and the channel offers an asymptotically favorable channel if

$$\frac{\mathbf{z}_k^H \mathbf{z}_l}{\sqrt{\mathbb{E}\{\|\mathbf{z}_k\|^2\}\mathbb{E}\{\|\mathbf{z}_l\|^2\}}} \to 0, \tag{37}$$

holds for any $k \neq l$. In real scenarios, for a finite number of M, N, the deterministic favorable propagation metric is defined as

$$\mathrm{FP}_{kl} = \frac{\mathrm{Var}\{\mathbf{z}_k^H \mathbf{z}_l\}}{\mathbb{E}\{\|\mathbf{z}_k\|^2\}\mathbb{E}\{\|\mathbf{z}_l\|^2\}}. \tag{38}$$

This property plays an important role especially in the uplink transmission because, if the channels are favorable, the transmitted signals from K users will belong to K orthogonal spaces. As a result, the BS can decode the signal sent by user k without inter-user interference, corresponding to the Maximum Ratio Combining (MRC) technique.

The **Channel Hardening** property is a phenomenon where the norm square of the aggregated channel vectors from the BS to the users does not fluctuate significantly, even when the small-scale fading channels randomly change. Mathematically, an aggregated channel offers channel hardening as $M, N \to \infty$, and if we have

$$\frac{\|\mathbf{z}_k\|^2}{\mathbb{E}\{\|\mathbf{z}_k\|^2\}} \to 1, \tag{39}$$

Since z_k is a random vector, it is nontrivial to exploit the 39 to prove the channel hardening property of the channels. In order to seek for a more tractable metric, we employ the Chebyshev inequality and we can reformulate for finite number of M, N and define the deterministic channel hardening property as

$$CH_k = \frac{\mathrm{Var}\left\{\|\mathbf{z}_k\|^2\right\}}{\left(\mathbb{E}\left\{\|\mathbf{z}_k\|^2\right\}\right)^2}. \tag{40}$$

we desire that $CH \to 0$ in real scenarios. If the channels harden, in the uplink, the BS can replace the instantaneous channel gain by its mean value for signal detection. This significantly simplifies the signal processing as well as resource allocation designs at the BS because all designs now can be done on the large-scale fading time scale. With TDD, the importance of channel hardening is even more significant in the downlink data transmission. In the downlink, thanks to the channel hardening property, each user can treat the mean value of the effective channel gain as the true one to detect the desired signal. Thus, no downlink pilot overhead is required for the downlink channel estimation.

E. Application of Reconfigurable Intelligent Surfaces

- Coverage extension
  RISs utilize the beamforming gain as they reflect the waves. The gain of the passive surfaces is proportional to N^2 in the SU-SISO system, and the corresponding equations are given by

  kamel beshe notation paiin az maghale review

  $G \sim \mathcal{CN}\left(0_N, \sigma_g^2 I_N\right)$, $H \sim \mathcal{CN}\left(0_N, \sigma_h^2 I_N\right)$,

$$SNR_{Passive} \sim N^2 \frac{P_{Tx}\pi^2\sigma_g^2\sigma_h^2}{16\sigma^2} \tag{41}$$

- Refining the channel Statistics properties
  Changing the channel characteristics, such as slow or fast fading or frequency-selective fading, to flat fading is possible.
- Interference suppression
  The controller that operates the surface always senses the channel and the transmission status. Thus, signal processing techniques can be deployed and transferred to RIS in order to suppress interference.
- Improving wireless channel rank
  Spatial correlation between transmitter elements in MIMO systems always exists.

  Reduce correlation by $\frac{\lambda}{2}$

  The condition number metric, defined as the ratio $\frac{\lambda_1}{\lambda_2}$, serves as an indicator of channel capacity. One application of RIS is to manipulate the channel to reduce the condition number, thereby improving system performance.

F. Optimization Objectives

There are many metrics that can be applied to the phase-shift matrix. The argument $\beta e^{j\theta_k}$ comprises the amplification and phase-shift of each element. Most methods for optimizing phase-shifts focus on optimizing the phase and setting $\beta = 1$.

G. Energy Efficiency

[14]

H. Sum-Rate optimization

manifold optimization cite Mérouane Debbah

IV. Problem Formulation

The RIS-assisted MIMO system in the far-field case is rank-deficient [15]. As the distance between the transmitter and receiver increases, the correlation between channels rises, and this phenomenon intensifies in indoor channels due to the presence of more clusters [16]. The correlation also depends on the number of multipath clusters and their angular locations [8].

inja hatman az channel hardening bayad estefade konim baraye tozihat rank

A. Preliminaries

m is the number of transmitters, and k is the number of antennas on the receiver side. The received vector $\mathbf{y} \in \mathbb{C}^k$, and the received signal is based on

$$\boldsymbol{y} = H\boldsymbol{x} + \boldsymbol{n} \tag{42}$$

where

$H = \mathbb{C}^{k\times m}$ and $\boldsymbol{n}$

is zero-mean complex Gaussian circularly symmetric noise. We assume $\mathbb{E}[\boldsymbol{n}\boldsymbol{n}^H] = I_m$ along with the noise received at each antenna is independent. The maximum transmitter power represents as

$$\mathbb{E}[\boldsymbol{x}^H\boldsymbol{x}] \leq P \tag{43}$$

likewise, Since $\boldsymbol{x}^H\boldsymbol{x} = tr(\mathbb{E}[\boldsymbol{x}\boldsymbol{x}^H])$ the above expression changes into,

$$\mathrm{tr}(\mathbb{E}[\boldsymbol{x}\boldsymbol{x}^H]) \leq P \tag{44}$$

B. Effective rank definition

The rank of a matrix A traditionally refers to the number of linearly independent rows or columns, or, in this context, the number of dimensions retained by the transformation (i.e., the dimension of the space spanned by the transformed vectors). This is purely a counting measure and does not provide information about the actual "shape" induced by the transformation. On the other hand, the effective rank goes beyond the binary definition of rank (nonzero versus zero singular values) by quantifying how much the transformation preserves and shapes different dimensions [17]. It achieves this by analyzing the spectral entropy of the distribution of singular values.

Example:

Assume a bi-dimensional Gaussian random vector with highly correlated components: The covariance matrix of this vector is said to have a rank of two (i.e., it spans two dimensions), but due to high correlation, most of the energy is concentrated along one direction (essentially collapsing one dimension). Thus, while the formal rank is two, the effective rank is slightly greater than one because one dimension is significantly more dominant than the other.

Calculation of Effective Rank:

Assume we have a matrix $A_{M\times N}$ whose singular value decomposition (SVD) is given by $A = U\Sigma V^H$, where $U_{M\times M}$ and $V_{N\times N}$ are unitary matrices, and $\Sigma_{M\times N}$ is a diagonal matrix containing the (real positive) singular values

$$\lambda_1 \geq \lambda_2 \geq \cdots \geq \lambda_Q \geq 0,$$

with $Q = \min\{M, N\}$ (representing the rank of the matrix), and $\lambda = (\lambda_1, \lambda_2, \ldots, \lambda_Q)^T$. Then, defining the normalized singular values are calculated through

$$\rho_k = \frac{\lambda_k}{\|\lambda\|_1}$$

$$\mathrm{erank}(A) = \exp\{H(\rho_1, \rho_2, \ldots, \rho_Q)\},$$

where $H(\rho_1, \rho_2, \ldots, \rho_Q)$ is the Shannon entropy given by:

$$H(\rho_1, \rho_2, \ldots, \rho_Q) = -\sum_{k=1}^{Q} \rho_k \log \rho_k.$$

In addition, the following inequality holds:

$$1 \leq \mathrm{erank}(A) \leq \mathrm{rank}(A) \leq Q.$$

In reference [10], the channel is defined in this way:

$$\mathbf{H} = \sqrt{\alpha} \underbrace{\mathbf{H\Theta G}}_{\text{RIS-assisted channel}} + \sqrt{1-\alpha} \left(\underbrace{\sqrt{\frac{K}{1+K}}\mathbf{H}_{\text{LoS}} + \sqrt{\frac{1}{1+K}}\mathbf{H}_{\text{NLoS}}}_{\text{non-RIS-assisted channel}} \right),$$

which is a combination of the RIS cascade channel, LOS, and NLOS channels. The problem is defined as follows:

$$\underset{\boldsymbol{\phi}}{\text{maximize}}\ \text{erank}(\mathbf{H}) \text{ subject to } \forall \phi_n \in \Xi_b,\ n = 1, 2, \ldots, N.$$

where erank is defines as:

$$\text{erank}(\mathbf{H}) = \exp\left(\sum_{i=1}^{\text{rank}(\mathbf{H})} -\rho_i \ln \rho_i \right),$$

C. Capacity analysis

Assume the matrix $H \in \mathbb{C}^{k\times m}$ exists. The singular value decomposition of the channel H is given by

$$H = U\Sigma V^H \tag{45}$$

where $U \in \mathbb{C}^{k\times k}$ and $V \in \mathbb{C}^{m\times m}$ are unitary matrices, and $\Sigma \in \mathbf{R}^{k\times m}$ is a real, non-negative, rectangular diagonal matrix. The diagonal entries of the matrix Σ are called singular values and are ordered as $\lambda_1 \geq \cdots \geq \lambda_{\min(k,m)} \geq 0$. Moreover the singular basis vectors of the SVD are orthonormal.

Generally, We can express the received signal at the receiver side for MIMO communication system wherein M transmitter antennas send the Q parallel data streams. The $Q \leq M$ is a representative of the rank of equivalent channel which is limited to the transmitter's antenna arrays. The signal will be shaped as they pass through the pre-coding and post-coding where $T \in \mathbb{C}^{M\times Q}$ and $R \in \mathbb{C}^{Q\times K}$ respectively.

$$y = \left(\sqrt{\frac{P}{Q}}\right) R(L + H\Theta G)Tx + n \tag{46}$$

The rate for 46 is given by

$$R = \log_2 \det\left(I + \frac{P}{\sigma^2 Q} H_{eq} T T^H H_{eq}^H \right). \tag{47}$$

The equivalent channel composed of Non line of sight and line of sight channels in the RIS-assisted system. The optimal solution for the pre-oding and post-coding are

$$R_{opt} = U^H \tag{48}$$

$$T_{opt} = V\hat{P}^{\frac{1}{2}} \tag{49}$$

The $\hat{\mathbf{P}}$ is formulated [18] as

$$\hat{\mathbf{P}} = \left[\text{diag}(p_1, \ldots, p_Q), \mathbf{0}_{Q\times(M-Q)}\right]^T \in \mathbb{R}^{M\times Q}, \tag{50}$$

and $p_q \geq 0$ denotes the corresponding stream power allocation. Furthermore, $q \in \mathcal{Q} = \{1, \ldots, Q\}$ and and the rate for each eigen-channel can be re-express as

$$\hat{R}_q = \log_2\left(1 + \frac{P_q \lambda_q^2}{\sigma^2 Q}\right) \tag{51}$$

which we can use water-filling algorithm in order to maximizing the sum-rate. The optimal power power allocation is given by

$$p_q = \max\left(\eta - \frac{\sigma^2 Q}{P\lambda_q^2}, 0\right), \tag{52}$$

D. Optimization of phase shift under Sum-path-gain maximization(SPGM) criterion

investigating the optimization problem under SPGM criterion which aims to maximize the sum of the eigen-channel gains [18]

$$\sum_{q=1}^{Q} \lambda_q^2 = \mathrm{tr}\left(H_{eq}^H H_{eq}\right) \tag{53}$$

is quite challenging due to the non convex form. Writing the objective function will help us find the optimal solution and elaborate more on this objection.

$$\max_{\boldsymbol{\theta}} \quad \psi(\boldsymbol{\theta}) = \mathrm{tr}\left[(\mathbf{L}+\mathbf{H}\boldsymbol{\Theta}\mathbf{G})^H(\mathbf{L}+\mathbf{H}\boldsymbol{\Theta}\mathbf{G})\right] \tag{54}$$

$$\text{s.t.} \quad [\boldsymbol{\Theta}]_{nn} = e^{j\theta_n}, \quad \forall n \in \mathcal{N}. \tag{55}$$

A self-developed algorithm, designated as 'Dimension-wise Sinusoidal Maximization'(DSM) is deployed to solve this problem.

$$\theta_{mn}^{(\mathrm{opt})} = \angle\left[\mathbf{H}^H\left(\mathbf{L}+\mathbf{H}\tilde{\boldsymbol{\Phi}}_{mn}\mathbf{G}\right)\mathbf{G}^H\right]_{mn}, \tag{56a}$$

$$\theta_{mn}^{(\mathrm{opt})} = \angle\left[\mathbf{H}^H\left(\mathbf{L}+\mathbf{H}\tilde{\boldsymbol{\Phi}}_{mn}\mathbf{G}\right)\mathbf{G}^H\right]_{mn} + \pi, \tag{56b}$$

$$\theta_n^{(i)} = \angle\left[l_{nn} + \sum_{\hat{n}=1}^{n-1} \exp\left(j\theta_{\hat{n}}^{(i)}\right) h_{n\hat{n}} g_{\hat{n}n} + \sum_{\hat{n}=n+1}^{N} \exp\left(j\theta_{\hat{n}}^{(i-1)}\right) h_{n\hat{n}} g_{\hat{n}n}\right], \tag{57}$$

where $l_{nn} \triangleq [\mathbf{H}^H\mathbf{L}\mathbf{G}^H]_{nn}$, $h_{n\hat{n}} \triangleq [\mathbf{H}^H\mathbf{H}]_{n\hat{n}}$, $g_{\hat{n}n} \triangleq [\mathbf{G}\mathbf{G}^H]_{\hat{n}n}$, $\forall n, \hat{n} \in \mathcal{N}$, and i denotes the iteration index.

Algorithm 1 Finding The Global Maximum of Problem

Require: $\mathbf{G}, \mathbf{H}, \mathbf{L}, P/\sigma^2$
Ensure: R
1: Initialize $i = 0$. Set an initial $\boldsymbol{\theta}$.
2: Compute $l_{nn} = [\mathbf{H}^H\mathbf{L}\mathbf{G}^H]_{nn}$, $h_{n\hat{n}} = [\mathbf{H}^H\mathbf{H}]_{n\hat{n}}$, and $g_{\hat{n}n} = [\mathbf{G}\mathbf{G}^H]_{\hat{n}n}$.
3: while $\left|\psi\left(\boldsymbol{\theta}^{(i)}\right) - \psi\left(\boldsymbol{\theta}^{(i-1)}\right)\right| > \epsilon$ do
4: Increase i.
5: for $n = 1 : N$ do
6: Update $\theta_n^{(i)}$ using (8).
7: end for
8: end while
9: Compute $\mathbf{H}_{\text{eff}} = \mathbf{L} + \mathbf{H}\boldsymbol{\Phi}\mathbf{G}$. $\mathbf{Q} = \mathrm{rank}(\mathbf{H}_{\text{eff}})$. Get $\mathbf{U}, \boldsymbol{\Sigma}, \mathbf{V}$ via SVD of $\mathbf{H}_{\text{eff}}$.
10: Obtain R by solving (3) with $\hat{P}$ as the variable of interest using WF procedure.

E. Optimizing the phase-shift of RIS using joint active and passive beamforming

nahve hal masale va optimized kardan rui zhang

Optimizing joint passive and active beamforming is a challenging topic. Notoriously, dealing with NP-hard problems is inevitable, and we must work on solving high-dimensional phase-shift matrices. In [9], the author's approach to tackle this problem combines Semi-Definite Relaxation and Variable Transformation. In addition, another technique named Alternative Optimization (AO) has been utilized to make this problem tractable and achieve lower complexity [9].

F. Multi User Energy Efficiency Optimization

They considered RIS-aided downlink communications in a single-cell network. The RIS is deployed in the channel to assist MU-MISO communication with K single-user antennas. Generally, there are two operation modes for RIS: the receiving mode for channel estimation and the reflecting mode for reflecting the incident wave [19]. Another assumption is that the AP has complete knowledge of the channel state information (CSI) for all channels. Furthermore, a quasi-static flat fading model is adopted for all channels. The time-division duplexing (TDD) protocol is considered for uplink and downlink transmission, with reciprocity for CSI acquisition in the downlink based on uplink training [9]. The complex baseband representation for the transmitted signal is shaped as $x = \sum_{k=1}^{K} w_k s_k$, where s_k and w_k denote the transmitted signal and beamforming vector at the AP, respectively.

Define the dimensions of x and w_k

The signal received at user k for both Non-Line of Sight (NLOS) and Line of Sight (LOS) paths is expressed as

$$y_k = (h_{r,k}\Theta\mathbf{G} + l_{d,k}) \sum_{j=1}^{K} w_j s_j + n_k, \quad k = 1, \ldots, K, \tag{58}$$

For simplicity, the noise is modeled as additive white Gaussian noise (AWGN). The SINR of user k is given by

$$\mathrm{SINR}_k = \frac{\left| \left(h_{r,k}^H \Theta\mathbf{G} + l_{d,k}^H \right) w_k \right|^2}{\sum_{j \neq k}^{K} \left| \left(h_{r,k}^H \Theta\mathbf{G} + l_{d,k}^H \right) w_j \right|^2 + \sigma_k^2}, \quad \forall k. \tag{59}$$

ghesmat problem formulation to copy konim inja

$$\text{(P1):} \quad \min_{\mathbf{w},\boldsymbol{\theta}} \sum_{k=1}^{K} \|w_k\|^2 \tag{60}$$

$$\text{s.t.} \quad \frac{|(\mathbf{h}_{r,k}\boldsymbol{\Theta}\mathbf{G} + \mathbf{h}_{d,k})\mathbf{w}_k|^2}{\sum_{j \neq k} |(\mathbf{h}_{r,k}\boldsymbol{\Theta}\mathbf{G} + \mathbf{l}_{d,k})\mathbf{w}_j|^2 + \sigma_k^2} \geq \gamma_k, \quad \forall k, \tag{61}$$

$$0 \leq \theta_n \leq 2\pi, \quad n = 1, \ldots, N, \tag{62}$$

where $\gamma_k > 0$ is the minimum required SNR for user k. Although problem 62 is convex, due to the non-convex constraint and coupling between the transmit signal and beamforming vector, there is no straightforward method to address this problem. The application of SDR and AO will be demonstrated in this section.

Proposition 1: For feasibility, this condition must be satisfied: $\mathrm{rank}(G^H H_r + l) = K$. Additionally, the (right) pseudo-inverse of $H^H = H^H \Theta G^H + l^H$ exists with $\Theta = I$, and the precoding matrix W at the AP can be set as $W = H(H^H H)^{-1}\mathrm{diag}(\gamma_1\sigma_1^2, \ldots, \gamma_k\sigma_k^2)^{\frac{1}{2}}$ to fulfill each user's required SINR.

Modifying (P1) to a single-user system is shown as follows:

$$\text{(P2):} \quad \min_{w,\theta} \quad \|w\|^2 \tag{63}$$

$$\text{s.t.} \quad |(h_r\Theta G + l)w|^2 \geq \gamma\sigma^2, \tag{64}$$

$$0 \leq \theta_n \leq 2\pi, \quad n = 1, \ldots, N. \tag{65}$$

1) SDR

Problem (P2) remains non-convex, and applying SDR would transform the problem into a relaxed form. The Maximum-Ratio Transmission (MRT) is the optimal beamforming solution for problem (P2) [20], i.e., $w^* = \sqrt{P}\frac{(h_r\Theta G + l)^H}{\|h_r\Theta G + l\|}$, where P denotes the transmit power of the AP. Substituting w^* simplifies problem (P2) to

$$\min_{P,\theta} \quad P \tag{66}$$
$$\text{s.t.} \quad P\|h_r\Theta G + l\|^2 \geq \gamma\sigma^2, \tag{67}$$
$$0 \leq \theta_n \leq 2\pi, \quad \forall n. \tag{68}$$

The optimal transmit power is $P^* = \frac{\gamma\sigma^2}{\|h_r\Theta G + l\|^2}$. In the same manner, minimizing the power is equivalent to maximizing the channel gain, i.e.,

$$\max_{\theta} \quad \|h_r\Theta G + l\|^2 \tag{69}$$
$$\text{s.t.} \quad 0 \leq \theta_n \leq 2\pi, \quad \forall n. \tag{70}$$

Let $v = [v_1, \ldots, v_N]^H$, where $v_n = e^{j\theta_n}$ for all n. Then, the constraints in 70 are equivalent to unit-modulus constraints, defined as: $|v_n|^2 = 1$ for all n. Changing variables as $h_r\Theta G = v^H\Phi$ where $\Phi = \text{diag}(h_r)G \in \mathbb{C}^{N\times M}$, yields $\|h_r\Theta G + l\|^2 = \|v^H\Phi + l\|^2$. Thus, problem 69 can be rewritten as

$$\max_{v} \quad v^H\Phi\Phi^H v + v^H\Phi l^H + l\Phi^H v + \|l\|^2 \tag{71}$$
$$\text{s.t.} \quad |v_n|^2 = 1, \quad \forall n. \tag{72}$$

It is noteworthy that problem 71 is a non-convex quadratically constrained quadratic program (QCQP). Reformulating it as a homogeneous QCQP [21] provides a more general representation form. Adding an auxiliary variable t to problem 71 yields the equivalent form:

$$\max_{\bar{v}} \quad \bar{v}^H\boldsymbol{R}\bar{v} + \|l\|^2 \tag{73}$$
$$\text{s.t.} \quad |\bar{v}_n|^2 = 1, \quad n = 1, \ldots, N+1, \tag{74}$$

where

$$\boldsymbol{R} = \begin{bmatrix} \Phi\Phi^H & \Phi l^H \\ l\Phi^H & 0 \end{bmatrix}, \quad \bar{v} = \begin{bmatrix} v \\ t \end{bmatrix}.$$

The problem 73 remains non-convex; however, defining $\bar{v}^H\boldsymbol{R}\bar{v} = \text{tr}(\boldsymbol{R}\bar{v}\bar{v}^H)$ and introducing $\boldsymbol{V} = \bar{v}\bar{v}^H$ leads to the constraints $\boldsymbol{V} \succeq 0$ and $\text{rank}(\boldsymbol{V}) = 1$. Since the rank-one constraint is non-convex, we apply SDR to relax the constraints. As a result, problem 73 reduces to

$$\max_{V} \quad \text{tr}(\boldsymbol{R}\boldsymbol{V}) + \|l\|^2 \tag{75}$$
$$\text{s.t.} \quad V_{n,n} = 1, \quad n = 1, \ldots, N+1, \tag{76}$$
$$\boldsymbol{V} \succeq 0. \tag{77}$$

The problem 75 is now formed as SDR and convex, it can be solved using a solver like CVX [22]. If the solution does not satisfy $\text{rank}(\boldsymbol{V}) = 1$, the optimal value should be interpreted as an upper-bound solution.

2) AO

The SDR approach's complexity is relatively high, so a less complex approach, Alternative Optimization (AO), may be considered. Let $w = \sqrt{P}\bar{w}$, where $\bar{w}$ represents the transmit beamforming direction and P denotes the transmit power. The (P2) problem is formulated as

$$\max_{\theta} \quad \left|\left(\mathbf{h}_r \Theta \mathbf{G} + l\right)\bar{\boldsymbol{w}}\right|^2 \tag{78}$$

$$\text{s.t.} \quad 0 \le \theta_n \le 2\pi, \quad n = 1, \ldots, N. \tag{79}$$

Like the previous problem, this one is also non-convex. Applying the triangle inequality, we have

$$\left|\left(\mathbf{h}_r \Theta \mathbf{G} + l\right)\bar{\boldsymbol{w}}\right| = \left|\mathbf{h}_r \Theta \mathbf{G}\bar{\boldsymbol{w}} + l\bar{\boldsymbol{w}}\right| \tag{80}$$

$$\overset{(a)}{\le} \left|\mathbf{h}_r \Theta \mathbf{G}\bar{\boldsymbol{w}}\right| + \left|l\bar{\boldsymbol{w}}\right|, \tag{81}$$

where equality holds if and only if $\arg\left(\mathbf{h}_r \Theta \mathbf{G}\bar{\boldsymbol{w}}\right) = \arg\left(l\bar{\boldsymbol{w}}\right) \triangleq \varphi_0$. Changing variables as $\boldsymbol{h_r}\Theta\mathbf{G}\boldsymbol{w} = \boldsymbol{v}^H\boldsymbol{a}$, where $\boldsymbol{v} = [e^{j\theta_1}, \ldots, e^{j\theta_N}]^H$ and $\boldsymbol{a} = \mathrm{diag}(\boldsymbol{h_r})\mathbf{G}\bar{\boldsymbol{w}}$, allows us to rewrite the objective function 78 as

$$\max_{\boldsymbol{v}} \quad \left|\boldsymbol{v}^H\boldsymbol{a}\right|^2 \tag{82}$$

$$\text{s.t.} \quad |v_n| = 1, \quad \forall n = 1, \ldots, N, \tag{83}$$

$$\arg\left(\boldsymbol{v}^H\boldsymbol{a}\right) = \varphi_0. \tag{84}$$

The optimal solution for 82 is given by $\boldsymbol{v^*} = e^{j(\varphi_0 - \arg(\boldsymbol{a}))} = e^{j(\varphi_0 - \arg(\mathrm{diag}((\boldsymbol{h_r^H})\mathbf{G}\bar{\boldsymbol{w}}))}$. Thus, the optimal phase shift of the n-th element of RIS is obtained by

$$\theta_n^* = \varphi_0 - \arg\left(\mathbf{h}_{n,r}\mathbf{g}_n^H\bar{\boldsymbol{w}}\right) \tag{85}$$

$$= \varphi_0 - \arg\left(\mathbf{h}_{n,r}\right) - \arg\left(\mathbf{g}_n^H\bar{\boldsymbol{w}}\right). \tag{86}$$

This algorithm shows that the obtained phase θ_n^* is independent of the amplitude of $h_{n,r}$. The optimal power is achieved by $P^* = \dfrac{\gamma\sigma^2}{\left\|\left(\mathbf{h}_r \Theta \mathbf{G} + l\right)\bar{\boldsymbol{w}}\right\|^2}$.

write untill section c

G. MIMO RIS phase shift optimization

[8] The capacity for MIMO system using channel H can be expressed as

$$C = \log_2\left(\det\left(\mathbf{I}_M + \frac{1}{N_0}\mathbf{H_{eq}}\mathbf{V}\mathbf{Q}^{\mathrm{opt}}\mathbf{V}^H{\mathbf{H_{eq}}}^H\right)\right). \tag{87}$$

We can introduce a new notation $\mathbf{H} = [h_1, \cdots, h_N]$ and $\mathbf{G} = [\vec{g}_1, \cdots, \vec{g}_N]^T$ where $\vec{h}_n$ is the nth row and the arrow notation points out that rows are horizontal. The $\mathbf{Q}_{opt}$ matrix contains all the optimal power allocation to antenna arrays at the transmitter side which has been solved by Water Filling algorithm. we can rewrite the equivalent channel as

$$\mathbf{H}_{eq} = L + H\Theta G = L + \sum_{i=1}^{N} h_i e^{j\theta_i}\vec{g}_i^T = \mathbf{H}_n + e^{j\theta_n}h_n\vec{g}_n^T \tag{88}$$

where $\mathbf{H}_n = L + \sum_{i=1, i\neq n}^{N} h_n e^{j\theta_i}\vec{g}_n^T$ contains all the terms except the specific phase θ_n. We do this to ensure that all the other phase shifts remain constant while we optimize the specific virtual path with the corresponding phase shift. Substituting 88 into 87 results in

$$\begin{aligned}
&\log_2\left(\det\left(\mathbf{I}_M + \frac{1}{N_0}\left(\mathbf{H}_n + e^{j\theta_n}\mathbf{h}_n\vec{g}_n^H\right)\mathbf{V}\mathbf{Q}^{\mathrm{opt}}\mathbf{V}^H\left(\mathbf{H}_n + e^{j\theta_n}\mathbf{h}_n\vec{g}_n^H\right)^H\right)\right),\\
&= \log_2\left(\det\left(\mathbf{A}_n + e^{j\theta_n}\mathbf{h}_n\mathbf{b}_n^H + e^{-j\theta_n}\mathbf{b}_n^H\mathbf{h}_n^H\right)\right),\\
&= \log_2\left(\det\left(\mathbf{A}_n\right)\right) + \log_2\left(\det\left(\mathbf{I}_M + e^{j\theta_n}\mathbf{A}_n^{-1}\mathbf{h}_n\mathbf{b}_n^H + e^{-j\theta_n}\mathbf{A}_n^{-1}\mathbf{b}_n^H\mathbf{h}_n^H\right)\right).
\end{aligned} \tag{89}$$

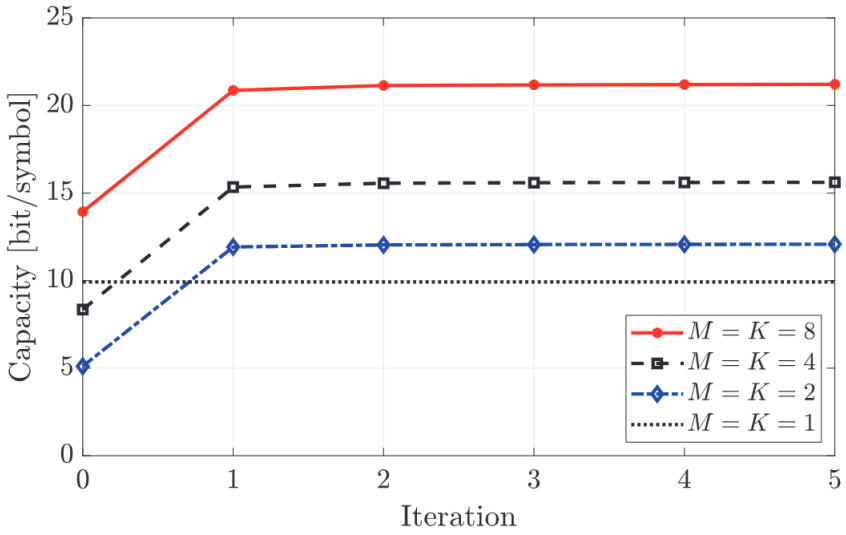

Figure 12: The point-to-point MIMO capacity enhancement through running the algorithm 2 for RIS-assisted system over multiple configurations

where we define these two variables

$$\mathbf{A}_n = \mathbf{I}_M + \frac{1}{N_0}\mathbf{H}_n\mathbf{V}\mathbf{Q}^{\text{opt}}\mathbf{V}^H\mathbf{H}_n^H + \frac{1}{N_0}\mathbf{h}_n\vec{g}_n^H\mathbf{V}\mathbf{Q}^{\text{opt}}\mathbf{V}^H\vec{g}_n^*\mathbf{h}_n^H \tag{90a}$$

$$\mathbf{b}_n = \frac{1}{N_0}\mathbf{H}_n\mathbf{V}\mathbf{Q}^{\text{opt}}\mathbf{V}^H\vec{g}_n^* \tag{90b}$$

The second determinant in 89 significantly impacts the optimization, so we can reformulate the second term as

$$\begin{aligned}
&\det\left(\mathbf{I}_M + \begin{bmatrix}\mathbf{A}_n^{-1}\mathbf{h}_n & \mathbf{A}_n^{-1}\mathbf{b}_n\end{bmatrix}\begin{bmatrix}e^{j\theta_n}\mathbf{b}_n^H \\ e^{-j\theta_n}\mathbf{h}_n^H\end{bmatrix}\right) \\
&= \det\left(\mathbf{I}_2 + \begin{bmatrix}e^{j\theta_n}\mathbf{b}_n^H & e^{-j\theta_n}\mathbf{h}_n^H\end{bmatrix}\begin{bmatrix}\mathbf{A}_n^{-1}\mathbf{h}_n & \mathbf{A}_n^{-1}\mathbf{b}_n\end{bmatrix}\right) \\
&= \left(1 + e^{j\theta_n}\mathbf{b}_n^H\mathbf{A}_n^{-1}\mathbf{h}_n\right)\left(1 + e^{-j\theta_n}\mathbf{h}_n^H\mathbf{A}_n^{-1}\mathbf{b}_n\right) - \mathbf{b}_n^H\mathbf{A}_n^{-1}\mathbf{b}_n\mathbf{h}_n^H\mathbf{A}_n^{-1}\mathbf{h}_n, \\
&= e^{j\theta_n}\mathbf{b}_n^H\mathbf{A}_n^{-1}\mathbf{h}_n + e^{-j\theta_n}\mathbf{h}_n^H\mathbf{A}_n^{-1}\mathbf{b}_n + \text{constants}.
\end{aligned} \tag{91}$$

The expression 91 is shaped based on Sylvester's Determinant Theorem as

$$\det(AB + I_M) = \det(BA + I_K) \tag{92}$$

In addition, the final expression in 91 will reach its maximum value if we choose

$$\psi_n = -\arg\left(\mathbf{b}_n^H\mathbf{A}n^{-1}\mathbf{h}n\right). \tag{93}$$

In conclusion, the algorithm is shown in Algorithm 2. For a few custom configurations the results over 6 iteration are shown in figure

Algorithm 2 Reconfigurable surface configuration for point-to-point MIMO capacity maximization.

1: Initialization: Set $\theta_1, \ldots, \theta_N$ randomly and select the number of iterations L.
2: for $i = 1, \ldots, L$ do
3: Compute the capacity-achieving covariance matrix $\mathbf{V}\mathbf{Q}^{\text{opt}}\mathbf{V}^H$ for the equivalent channel matrix with $\mathbf{D}_\theta = \text{diag}(e^{j\theta_1}, \ldots, e^{j\theta_N})$.
4: for $n = 1, \ldots, N$ do
5: Compute $\mathbf{A}_n$ in 90a and $\mathbf{b}_n$ in 90b for fixed $\theta_1, \ldots, \theta_N$.
6: $\theta_n \leftarrow -\arg\left(\mathbf{b}_n^H\mathbf{A}_n^{-1}\mathbf{h}_n\right)$.
7: end for
8: end for
9: Output: $\theta_1, \ldots, \theta_N$.

Gramma check end

V. Proposed Method

VI. Simulation Results or Evaluation of the Proposed Method

VII. Conclusion

The conclusion goes here.

Appendix A

Appendix one text goes here.

Appendix B

Appendix two text goes here.

Acknowledgment

The authors would like to thank...

References

[1] M. Di Renzo, A. Zappone, M. Debbah, M.-S. Alouini, C. Yuen, J. de Rosny, and S. Tretyakov, "Smart radio environments empowered by reconfigurable intelligent surfaces: How it works, state of research, and the road ahead," IEEE Journal on Selected Areas in Communications, vol. 38, no. 11, pp. 2450–2525, 2020.
[2] Z. Zhang, L. Dai, X. Chen, C. Liu, F. Yang, R. Schober, and H. V. Poor, "Active ris vs. passive ris: Which will prevail in 6g?" IEEE Transactions on Communications, vol. 71, no. 3, pp. 1707–1725, 2023.
[3] W. Tang, M. Z. Chen, X. Chen, J. Y. Dai, Y. Han, M. Di Renzo, Y. Zeng, S. Jin, Q. Cheng, and T. J. Cui, "Wireless communications with reconfigurable intelligent surface: Path loss modeling and experimental measurement," IEEE Transactions on Wireless Communications, vol. 20, no. 1, pp. 421–439, 2021.
[4] S. Abeywickrama, R. Zhang, and C. Yuen, "Intelligent reflecting surface: Practical phase shift model and beamforming optimization," in ICC 2020 - 2020 IEEE International Conference on Communications (ICC), 2020, pp. 1–6.
[5] Q. Wu and R. Zhang, "Beamforming optimization for wireless network aided by intelligent reflecting surface with discrete phase shifts," IEEE Transactions on Communications, vol. 68, no. 3, pp. 1838–1851, 2020.
[6] E. Björnson and L. Sanguinetti, "Rayleigh fading modeling and channel hardening for reconfigurable intelligent surfaces," IEEE Wireless Communications Letters, vol. 10, no. 4, pp. 830–834, 2021.
[7] T. L. Marzetta, E. G. Larsson, H. Yang, and H. Q. Ngo, Fundamentals of massive MIMO. Cambridge University Press, 2016.
[8] E. Björnson and Özlem Tuğfe Demir, Introduction to Multiple Antenna Communications and Reconfigurable Surfaces. Now Publishers, 2024.
[9] Q. Wu and R. Zhang, "Intelligent reflecting surface enhanced wireless network via joint active and passive beamforming," IEEE Transactions on Wireless Communications, vol. 18, no. 11, pp. 5394–5409, 2019.
[10] S. Meng, W. Tang, W. Chen, J. Lan, Q. Y. Zhou, Y. Han, X. Li, and S. Jin, "Rank optimization for mimo channel with ris: Simulation and measurement," IEEE Wireless Communications Letters, vol. 13, no. 2, pp. 437–441, 2024.
[11] M. Najafi, V. Jamali, R. Schober, and H. V. Poor, "Physics-based modeling of large intelligent reflecting surfaces for scalable optimization," pp. 559–563, 2020.
[12] J. Yang, Y. Chen, M. Jian, J. Dou, and M. Fang, "Capacity improvement in reconfigurable intelligent surface assisted mimo communications," IEEE Access, vol. 9, pp. 137 460–137 469, 2021.
[13] T. V. Chien, H. Q. Ngo, S. Chatzinotas, and B. Ottersten, "Reconfigurable intelligent surface-assisted massive mimo: Favorable propagation, channel hardening, and rank deficiency [lecture notes]," IEEE Signal Processing Magazine, vol. 39, no. 3, pp. 97–104, 2022.
[14] C. Huang, A. Zappone, G. C. Alexandropoulos, M. Debbah, and C. Yuen, "Reconfigurable intelligent surfaces for energy efficiency in wireless communication," IEEE Transactions on Wireless Communications, vol. 18, no. 8, pp. 4157–4170, 2019.
[15] J. Yang, Y. Chen, M. Jian, J. Dou, and M. Fang, "Capacity improvement in reconfigurable intelligent surface assisted mimo communications," IEEE Access, vol. 9, pp. 137 460–137 469, 2021.
[16] E. Basar, I. Yildirim, and F. Kilinc, "Indoor and outdoor physical channel modeling and efficient positioning for reconfigurable intelligent surfaces in mmwave bands," IEEE Transactions on Communications, vol. 69, no. 12, pp. 8600–8611, 2021.
[17] O. Roy and M. Vetterli, "The effective rank: A measure of effective dimensionality," in 2007 15th European Signal Processing Conference, 2007, pp. 606–610.
[18] A. Sirojuddin, D. D. Putra, and W.-J. Huang, "Low-complexity sum-capacity maximization for intelligent reflecting surface-aided mimo systems," IEEE Wireless Communications Letters, vol. 11, no. 7, pp. 1354–1358, 2022.
[19] L. Subrt and P. Pechac, "Intelligent walls as autonomous parts of smart indoor environments," IET Communications, vol. 6, pp. 1004–1010, 2012. [Online]. Available: https://digital-library.theiet.org/doi/abs/10.1049/iet-com.2010.0544
[20] D. Tse and P. Viswanath, Fundamentals of wireless communication. Cambridge university press, 2005.
[21] A. M.-C. So, J. Zhang, and Y. Ye, "On approximating complex quadratic optimization problems via semidefinite programming relaxations," Mathematical Programming, vol. 110, no. 1, pp. 93–110, 2007.
[22] M. Grant and S. Boyd, "CVX: Matlab software for disciplined convex programming, version 2.1," https://cvxr.com/cvx, Mar. 2014.